Letters

A Reconfigurable Rectifier Based Communication-Free Wireless LED Driver With Dual-Customization CC Outputs

Lin Yang, Yilin Wang, Pilong Guo, Kangshuai Dong, and Changsong Cai, *Senior Member, IEEE*

***Abstract*—Due to the advantages of safety and convenience, wireless power transfer technology is a good candidate for underwater LEDs driving. A wireless LED driver with a single constant current (CC) output value cannot enable LEDs to achieve brightness variation. This letter proposes a reconfigurable rectifier based communication-free wireless LED driver with dual-customization CC outputs. By simply controlling the special rectifier on the receiver, the proposed driver can be selectively configured into two LCC-S-S three-coil structures with different specifications, allowing LEDs to work in energy-saving mode and lighting mode, respectively. In addition, the control unit for mode switching is located at the receiver, making the system communication-free and ideal for underwater LEDs driving. An experimental prototype with dual-customization CC outputs of 0.6 A for energy-saving mode and 1 A for lighting mode is fabricated to verify the feasibility of the proposed wireless LED driver.**

***Index Terms*—Constant current (CC), dual-customization, special rectifier, wireless power transfer (WPT).**

I. Introduction

LEDS are widely used in general lighting, LCD lighting, and emergency lighting due to the advantages such as energy-saving and environmental protection [1]. When LEDs work underwater, it is more appropriate to choose a wireless power transfer (WPT) system to drive LED strings. A stable constant current (CC) source is the prerequisite for ensuring stable performance of LED strings [2]. Currently, researchers have proposed a variety of methods to achieve CC characteristic. The authors in [3] and, [4] adopted the phase shift control to enable the WPT system to perform CC output. However, this method is complex to control and difficult to achieve zero voltage switching (ZVS) operation. Introducing an additional dc–dc converter is also an alternative method to achieve CC output [5], [6]. However, this method will cause high system manufacturing cost, bulky size, etc. To overcome the shortcomings of the above methods, a variety of CC-type topologies have been proposed, such as LC^2-S in [7], LC-S in [8], and S-CLC in [9]. However, in some special scenarios, a single lighting brightness cannot meet special application requirements. During the day, when the swimming pool is well-lit, the system needs to provide a small current to drive LED strings to work in energy-saving mode to increase the swimming pool atmosphere and visual effects. At night or on cloudy days, when the light in the swimming pool is not sufficient, the system needs to provide a large current to drive LED strings to work in lighting mode to enhance brightness. Therefore, the above systems with a single CC output value cannot meet certain special requirements.

To solve the problems of complex control in [3] and [4], high manufacturing cost and bulky size in [5] and [6], and inability to provide two different specifications of CC output in [3], [4], [5], [6], [7], [8], and [9], this letter proposes a reconfigurable rectifier based wireless LED driver with dual-customization CC outputs. By controlling the working state of the MOSFETs in the special rectifier, the proposed driver can be configured into two LCC-S-S three-coil structures with different specifications to selectively drive LED strings to work in energy-saving mode or lighting mode. In addition, since the controller for mode switching is located at the receiver, the proposed driver does not require communication links and is very suitable for underwater LEDs driving.

II. Theoretical Analysis

A. Overview of the Proposed Wireless LED Driver

Fig. 1 shows the overall structure diagram of the proposed wireless LED driver. U_D is the dc input voltage. The inverter consists of four MOSFETs (Q_1–Q_4). L_1, L_P, L_S, and L_T, respectively, represent the inductor coils used in the proposed driver. C_1, C_P, C_S, and C_T, respectively, represent the compensation capacitors. M_{PT}, M_{PS}, M_{TS} represent the corresponding mutual inductances. $\boldsymbol{I}_1$–$\boldsymbol{I}_4$ represent the current phasors flowing through the corresponding coils, respectively. The yellow shaded part is the special rectifier consisting of a diode D_1 and two

Received 26 June 2024; revised 25 August 2024 and 24 September 2024; accepted 16 October 2024. Date of publication 28 October 2024; date of current version 18 December 2024. This work was supported in part by the National Natural Science Foundation of China under Grant 52207013 and in part by the Key Research Program of Higher Education of Henan under Grant 23A470007. *(Corresponding author: Changsong Cai.)*

Lin Yang, Yilin Wang, and Kangshuai Dong are with the College of Electronic and Electrical Engineering, The Academician Workstation of Electromagnetic Wave Engineering of Henan Province, Henan Normal University, Xinxiang 453007, China (e-mail: yang_lin@whu.edu.cn; wangyilin202282@stu.htu.edu.cn; dongkangshuai@stu.htu.edu.cn).

Pilong Guo and Changsong Cai are with the Hubei Key Laboratory of Power Equipment & System Security for Integrated Energy, School of Electrical Engineering and Automation, Wuhan University, Wuhan 430072, China (e-mail: pilongguo@whu.edu.cn; changsongcai@whu.edu.cn).

Color versions of one or more figures in this article are available at https://doi.org/10.1109/TPEL.2024.3487170.

Digital Object Identifier 10.1109/TPEL.2024.3487170

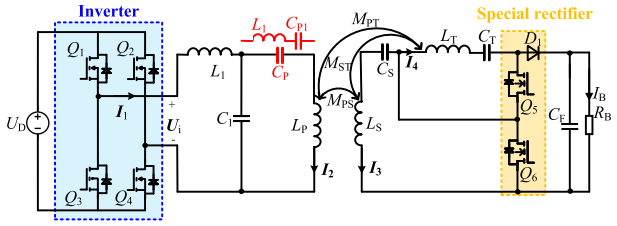

Fig. 1. Overall structure diagram of the proposed wireless LED driver.

TABLE I
CONTROL LOGIC OF THE SPECIAL RECTIFIER

Working mode	MOSFET Q_5	MOSFET Q_6
Energy-saving mode	Off	On
Lighting mode	On	Off

MOSFETs Q_5 and Q_6. By simply controlling the working states of the MOSFETs Q_5 and Q_6, the special rectifier can be suspended in different resonant loops, thereby reconstructing the wireless LED driver into two different LCC-S-S compensated three-coil structures. Through reasonable parameter design, the two three-coil structures can achieve two different CC outputs through their inherent structural properties, thereby realizing both the energy-saving mode and the lighting mode without the need for complex closed-loop control technology. The control logic of the special rectifier is provided in Table I. When MOSFET Q_5 is OFF and Q_6 is ON, the antiparallel diode of Q_5 together with diode D_1 forms the rectifier and the proposed driver operates in energy-saving mode. When MOSFET Q_5 is ON and Q_6 is OFF, the antiparallel diode of Q_6 together with diode D_1 forms the rectifier and the proposed driver operates in lighting mode.

To facilitate analysis, capacitor C_P is equivalent to an inductor L_1 and a capacitor C_{P1}, as shown in the red part of Fig. 1. After the equivalent, the proposed LCC-S-S compensated three-coil structure can be regarded as a cascade of a front-stage T network and a rear-stage S-S-S compensated three-coil structure. According to the T network characteristics in [10] and [11] and the S-S-S compensated three-coil structure characteristics in [12], when (1) is satisfied, the constant voltage (CV) source provided by the inverter can be transformed into a CC source through the T network. In addition, the S-S-S compensated three-coil structure can achieve CC output when powered by a CC source provided by the front-stage T network. Therefore, the proposed LCC-S-S compensated three-coil structure can achieve CC output function.

$$\begin{cases} C_1 = \left(\omega^2 L_1\right)^{-1}, C_S = \left(\omega^2 L_S\right)^{-1}, C_T = \left(\omega^2 L_T\right)^{-1} \\ C_{\mathrm{P1}} = \frac{M_{ST}}{\omega^2\left(L_P M_{ST} - 2M_{PT}M_{PS}\right)}. \end{cases} \tag{1}$$

Further, substituting $j\omega L_1 + 1/j\omega C_{\mathrm{P1}} = 1/j\omega C_{\mathrm{P}}$ into (1), C_P can be calculated as

$$C_{\mathrm{P}} = \frac{M_{ST}}{\omega^2\left(L_P M_{ST} - M_{ST}L_1 - 2M_{PT}M_{PS}\right)}. \tag{2}$$

The following will provide a more detailed theoretical analysis of the CC output and the corresponding zero phase angle (ZPA) operation characteristics in energy-saving mode and lighting mode.

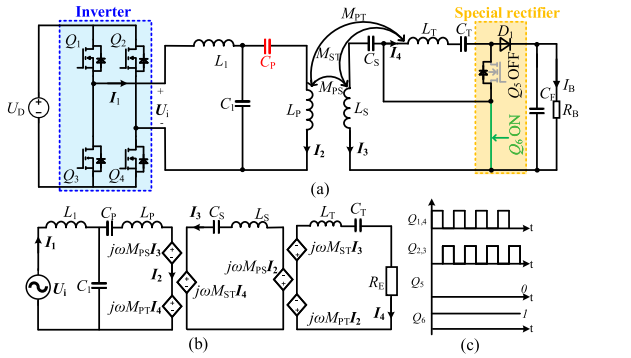

Fig. 2. Proposed wireless LED driver working in energy-saving mode. (a) Structure diagram. (b) Equivalent circuit diagram. (c) Switching timing diagram.

B. First CC Mode—Energy Saving Mode Analysis

In energy-saving mode, MOSFET Q_5 is OFF and Q_6 is ON, the antiparallel diode of Q_5 together with diode D_1 forms the rectifier suspended in the resonant loop composed of coil L_T and compensation capacitor C_T, and the driver is configured as a three-coil structure of the first specification to drive LED strings to work in energy-saving mode. In energy-saving mode, the loop composed of L_T and C_T is the receiving resonant circuit, and the loop composed of L_S and C_S is the relay resonant circuit. The structure diagram, equivalent circuit diagram, and switching timing diagram of the wireless LED driver working in energy-saving mode are shown in Fig. 2. The equivalent relationship between U_D and the root mean square value of the ac output voltage $\boldsymbol{U_i}$ of the inverter is shown in (3).

$$U_{\mathrm{i}} = \frac{2\sqrt{2}}{\pi} U_{\mathrm{D}}. \tag{3}$$

According to Kirchhoff's voltage law (KVL), the loop voltage expressions in Fig. 2(b) can be expressed as

$$\begin{cases} \left(j\omega L_1 + \frac{1}{j\omega C_1}\right)\boldsymbol{I}_1 - \frac{1}{j\omega C_1}\boldsymbol{I}_2 = \boldsymbol{U}_{\mathrm{i}} \\ -\frac{1}{j\omega C_1}\boldsymbol{I}_1 + \left(j\omega L_P + \frac{1}{j\omega C_1} + \frac{1}{j\omega C_P}\right)\boldsymbol{I}_2 \\ \quad + j\omega M_{\mathrm{PS}}\boldsymbol{I}_3 + j\omega M_{\mathrm{PT}}\boldsymbol{I}_4 = 0 \\ \left(j\omega L_S + \frac{1}{j\omega C_S}\right)\boldsymbol{I}_3 + j\omega M_{\mathrm{SP}}\boldsymbol{I}_2 + j\omega M_{\mathrm{ST}}\boldsymbol{I}_4 = 0 \\ \left(j\omega L_T + \frac{1}{j\omega C_T} + R_E\right)\boldsymbol{I}_4 + j\omega M_{\mathrm{ST}}\boldsymbol{I}_3 + j\omega M_{\mathrm{PT}}\boldsymbol{I}_2 = 0. \end{cases} \tag{4}$$

Substituting (1) and (2) into (4) and (5) can be solved as

$$\boldsymbol{I_4} = \frac{-\boldsymbol{U_i} M_{PS}}{j\omega L_1 M_{ST}}, Z_{in} = \frac{\boldsymbol{U_i}}{\boldsymbol{I_1}} = \frac{\omega^2 L_1^2 M_{ST}^2}{M_{PS}^2 R_E}. \tag{5}$$

According to (3) and (5), the output current I_{B1} of the wireless LED driver in energy-saving mode can be derived as

$$I_{\mathrm{B1}} = \frac{\sqrt{2}}{\pi} I_4 = \frac{4}{\pi^2}\frac{M_{PS} U_{\mathrm{D}}}{\omega L_1 M_{ST}}. \tag{6}$$

As evident from (5) and (6), the proposed wireless LED driver can achieve CC output and ZPA operation in energy-saving mode.

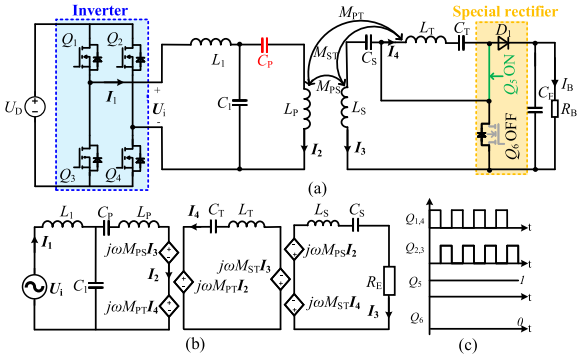

Fig. 3. Proposed wireless LED driver working in lighting mode. (a) Structure diagram. (b) Equivalent circuit diagram. (c) Switching timing diagram.

C. Second CC Mode—Lighting Mode Analysis

In lighting mode, MOSFET Q_5 is ON and Q_6 is OFF, the antiparallel diode of Q_6 together with diode D_1 forms the rectifier suspended in the resonant loop composed of coil L_S and compensation capacitor C_S, and the driver is configured as a three-coil structure of the second specification to drive LED strings to work in lighting mode. In lighting mode, the loop composed of L_S and C_S is the receiving resonant circuit, and the loop composed of L_T and C_T is the relay resonant circuit. The structure diagram, equivalent circuit diagram, and switching timing diagram of the wireless LED driver working in lighting mode are shown in Fig. 3. Based on KVL, (7) can be obtained as

$$\begin{cases} \left(j\omega L_1+\frac{1}{j\omega C_1}\right)\boldsymbol{I}_1-\frac{1}{j\omega C_1}\boldsymbol{I}_2=\boldsymbol{U}_{\rm i} \\ -\frac{1}{j\omega C_1}\boldsymbol{I}_1+\left(j\omega L_P+\frac{1}{j\omega C_1}+\frac{1}{j\omega C_P}\right)\boldsymbol{I}_2 \\ \quad +j\omega M_{\rm PS}\boldsymbol{I}_3+j\omega M_{\rm PT}\boldsymbol{I}_4=0 \\ \left(j\omega L_S+\frac{1}{j\omega C_S}+R_E\right)\boldsymbol{I}_3+j\omega M_{\rm SP}\boldsymbol{I}_2+j\omega M_{\rm ST}\boldsymbol{I}_4=0 \\ \left(j\omega L_T+\frac{1}{j\omega C_T}\right)\boldsymbol{I}_4+j\omega M_{\rm ST}\boldsymbol{I}_3+j\omega M_{\rm PT}\boldsymbol{I}_2=0. \end{cases} \tag{7}$$

Substituting (1) and (2) into (7) and (8) can be obtained as

$$\boldsymbol{I_3}=\frac{-\boldsymbol{U}_{\rm i}M_{PT}}{j\omega L_1 M_{ST}}, Z_{in}=\frac{\boldsymbol{U_i}}{\boldsymbol{I_1}}=\frac{\omega^2 L_1^2 M_{ST}^2}{M_{PT}^2 R_E}. \tag{8}$$

Similar to energy-saving mode, the output current I_{B2} in lighting mode can be derived as

$$I_{\rm B2}=\frac{\sqrt{2}}{\pi}I_3=\frac{4}{\pi^2}\frac{M_{PT}U_{\rm D}}{\omega L_1 M_{ST}}. \tag{9}$$

As evident from (8) and (9), the proposed wireless LED driver can achieve CC output and ZPA operation in lighting mode.

III. Experimental Verification

The feasibility of the proposed wireless LED driver is verified by constructing a validation experimental prototype, as shown in Fig. 4. Two LED strings with the specifications of $LED_{2\times8}$ and $LED_{2\times12}$ are used to evaluate the performance. The experimental parameters of the proposed driver are listed in Table II.

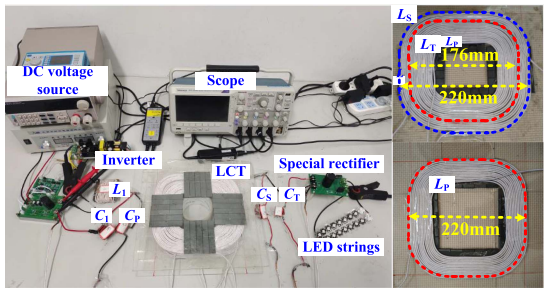

Fig. 4. Experimental prototype.

TABLE II
Experimental Parameters of the Proposed Wireless LED Driver

Parameters	Value	Parameters	Value	Parameters	Value
$U_{\rm D}$	20 V	L_1	20 μH	C_1	175.3 nF
$C_{\rm P}$	130 nF	$L_{\rm P}$	90.37 μH	$L_{\rm S}$	22.74 μH
$C_{\rm S}$	154.08 nF	$L_{\rm T}$	65.95 μH	$C_{\rm T}$	53.16 nF
$M_{\rm PS}$	16.7 μH	$M_{\rm PT}$	28 μH	$M_{\rm ST}$	21 μH
f	85 kHz	$I_{\rm B1}$	0.6 A	$I_{\rm B2}$	1 A

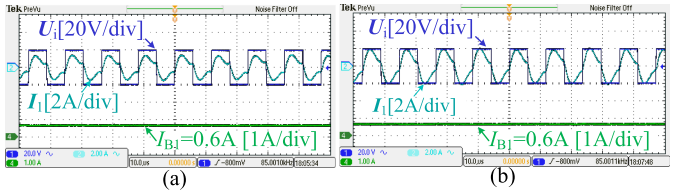

Fig. 5. Experimental waveforms of $\boldsymbol{U}_{\rm i}$, $\boldsymbol{I}_1$, and $I_{\rm B1}$ when the wireless LED driver working in energy-saving mode. (a) $LED_{2\times8}$ and (b) $LED_{2\times12}$.

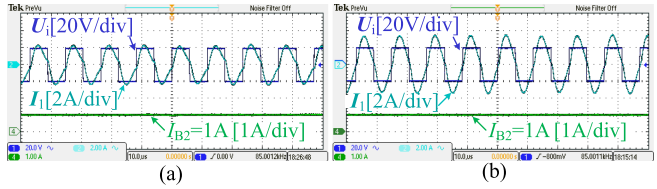

Fig. 6. Experimental waveforms of $\boldsymbol{U}_{\rm i}$, $\boldsymbol{I}_1$, and $I_{\rm B2}$ when the wireless LED driver working in lighting mode. (a) $LED_{2\times8}$ and (b) $LED_{2\times12}$.

$C_{\rm P}$ is intentionally slightly reduced to achieve ZVS operation of the proposed wireless LED driver.

When MOSFET Q_5 is turned OFF and Q_6 is turned ON, the proposed driver works in energy-saving mode. The measured waveforms corresponding to the two specifications of LED strings are shown in Fig. 5. The output current $I_{\rm B1}$ of the proposed wireless LED driver is maintained at 0.6 A regardless of the specifications of the connected LED strings. Meanwhile, $\boldsymbol{U}_{\rm i}$ slightly leads $\boldsymbol{I}_1$, which proves that the proposed driver can achieve approximately ZPA and ZVS operations in energy-saving mode.

When MOSFET Q_5 is turned ON and Q_6 is turned OFF, the proposed driver works in lighting mode. The measured waveforms corresponding to the two specifications of LED strings are shown in Fig. 6. The output current $I_{\rm B2}$ of the proposed wireless LED driver is maintained at 1 A regardless of the specifications of the connected LED strings. In addition, $\boldsymbol{U}_{\rm i}$ slightly leads $\boldsymbol{I}_1$,

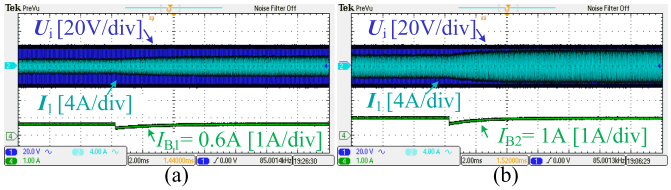

Fig. 7. Transition waveforms when the specifications of LED strings change suddenly from $LED_{2\times8}$ to $LED_{2\times12}$. (a) Energy-saving mode. (b) Lighting mode.

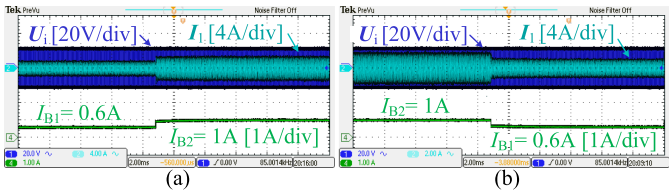

Fig. 8. Transition waveforms when the energy-saving mode and the lighting mode are interchanged. (a) Adopting the specification of $LED_{2\times8}$ from energy-saving mode to the lighting mode. (b) Adopting the specification of $LED_{2\times12}$ from lighting mode to the energy-saving mode.

which proves that the proposed driver can achieve nearly ZPA and ZVS operations in lighting mode.

Fig. 7 displays the transition waveforms when the specifications of LED strings change suddenly from $LED_{2\times8}$ to $LED_{2\times12}$ in the energy-saving mode and the lighting mode. As evident from Fig. 7(a) and (b), the output current $I_{\rm B1}$ in energy-saving mode and the output current $I_{\rm B2}$ in lighting mode does not fluctuate significantly before and after the specifications of LED strings change, which proves the stability of the proposed wireless LED driver.

Further, the transition process when the energy-saving mode and the lighting mode are interchanged is measured, as shown in Fig. 8. When MOSFET Q_5 changes from OFF to ON and Q_6 changes from ON to OFF, the transition waveforms adopting the specification of $LED_{2\times8}$ from the energy-saving mode to the lighting mode is displayed in Fig. 8(a). From Fig. 8(a), the output current of the proposed wireless LED driver is successfully converted from 0.6 A for the energy-saving mode to 1 A for the lighting mode. When MOSFET Q_5 changes from ON to OFF and Q_6 changes from OFF to ON, the transition waveforms adopting the specification of $LED_{2\times12}$ from lighting mode to the energy-saving mode is displayed in Fig. 8(b). From Fig. 8(b), the output current of the proposed wireless LED driver is successfully converted from 1 A for the lighting mode to 0.6 A for the energy-saving mode. The above experiments further demonstrate the safety and effectiveness of the proposed wireless LED driver.

Fig. 9 shows the dc–dc efficiency of the proposed wireless LED driver connected to different LED string specifications under energy-saving mode and lighting mode conditions, respectively. It can be seen from Fig. 9 that in both modes, the overall efficiency of the proposed driver is maintained at a high level.

The loss distribution of the proposed wireless LED driver at the peak efficiency point in energy-saving mode and lighting mode is depicted in Fig. 10. As evident from Fig. 10, the power dissipated in the rectifier, inverter, and loosely coupled transformer (LCT) accounts for the majority of the total losses in both energy-saving mode and lighting mode. Therefore, optimizing the design of rectifier, inverter, and LCT can further improve system efficiency.

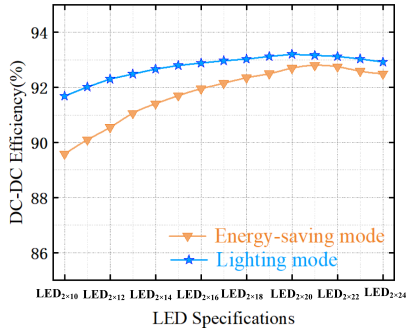

Fig. 9. DC–DC efficiency of the proposed wireless LED driver connected to different LED string specifications.

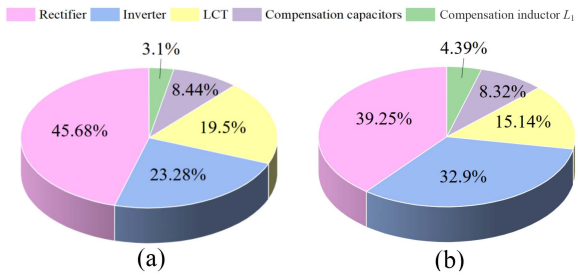

Fig. 10. Loss distribution of the proposed wireless LED driver at the peak efficiency point in (a) energy-saving mode and (b) lighting mode.

IV. Conclusion

Considering some special application requirements, this letter proposes a reconfigurable rectifier based communication-free wireless LED driver with dual-customization CC outputs. By controlling the working state of the MOSFETs in the special rectifier, the driver can be configured into two specifications of three-coil structure to drive LED strings to work in lighting mode or energy-saving mode, respectively. Meanwhile, the inverter is capable of approximate ZPA and ZVS operations, which ensures the high transfer efficiency. Furthermore, the communication-free feature makes the driver very suitable for underwater LEDs driving.

References

[1] S. Li, S. C. Tan, C. K. Lee, E. Waffenschmidt, S. Y. Hui, and C. K. Tse, "A survey, classification, and critical review of light-emitting diode drivers," *IEEE Trans. Power Electron.*, vol. 33, no. 5, pp. 4523–4534, May 2018.

[2] Y. Li, J. Hu, X. Li, H. Wang, and K. W. E. Cheng, "Cost-effective and compact multistring LED driver based on a three-coil wireless power transfer system," *IEEE Trans. Power Electron.*, vol. 33, no. 9, pp. 8065–8080, Sep. 2018.

[3] I. W. Iam et al., "Constant-frequency and NoncommunicationBased inductive power transfer converter for battery charging," *IEEE J. Emerg. Sel. Topics Power Electron.*, vol. 10, no. 2, pp. 2147–2162, Apr. 2022.

[4] K. Song, Z. Li, J. Jiang, and C. Zhu, "Constant current/voltage charging operation for series–series and series–parallel compensated wireless power transfer systems employing primary-side controller," *IEEE Trans. Power Electron.*, vol. 33, no. 9, pp. 8065–8080, Sep. 2018.

[5] Z. Huang, S. C. Wong, and C. K. Tse, "Control design for optimizing efficiency in inductive power transfer systems," *IEEE Trans. Power Electron.*, vol. 33, no. 5, pp. 4523–4534, May 2018.

[6] Z. Li, C. Zhu, J. Jiang, and G. Wei, "A 3-kW wireless power transfer system for sightseeing car supercapacitor charge," *IEEE Trans. Power Electron.*, vol. 32, no. 5, pp. 3301–3316, May 2017.

[7] Y. Zhang, H. Tang, Z. Shen, Y. Zhuang, and Z. Li, "An LC squared-compensated inductive power transfer system with misalignment tolerance and constant-current output," *IEEE Trans. Power Electron.*, vol. 39, no. 4, pp. 4850–4857, Apr. 2024.

[8] Y. Wang, Y. Yao, X. Liu, D. Xu, and L. Cai, "An LC/S compensation topology and coil design technique for wireless power transfer," *IEEE Trans. Power Electron.*, vol. 33, no. 3, pp. 2007–2025, Mar. 2018.

[9] C. Cai, J. Wang, M. Saeedifard, P. Zhang, R. Chen, and J. Zhang, "Gyrator-gain variable WPT topology for MC-Unconstrained CC output customization using simplified capacitance tuning," *IEEE Trans. Ind. Electron.*, vol. 71, no. 4, pp. 3594–3605, Apr. 2024.

[10] X. Qu, Y. Jing, H. Han, S.-C. Wong, and C. K. Tse, "Higher order compensation for inductive-power-transfer converters with constant-voltage or constant-current output combating transformer parameter constraints," *IEEE Trans. Power Electron.*, vol. 32, no. 1, pp. 394–405, Jan. 2017.

[11] Q. Wang et al., "Inductive power transfer system with constant current-constant voltage charging tolerating misalignment based on multi-objective optimization for compensation topology," *IEEE Trans. Power Electron.*, early access, doi: 10.1109/TPEL.2024.3435424.

[12] L. Yang, X. Li, S. Liu, Z. Xu, C. Cai, and P. Guo, "Analysis and design of three-coil analysis and design of three-coil structure WPT system with constant output currents," *IEEE Access*, vol. 7, pp. 87334–87344, 2019.